Activity and kinematic behaviors of gravitational slope deformation in the slate belt of Taiwan

Cheng-Han Lin
Department of Civil Engineering, National Taiwan University, Taipei, Taiwan

Ming-Lang Lin
Department of Civil Engineering, National Taiwan University, Taipei, Taiwan

ABSTRACT: In the slate belt of Taiwan, there have been numerous studies exploring landslide activity or gravitational slope deformation (GSD) since the 2009 Typhoon Morakot. However, studies evaluating the relationship between present-day activity and long-term deformation have been infrequent due to a lack of multi-temporal monitoring data and analysis tools. The Chingjing region, which contains many GSDs and famous rockslides, is one such region that requires further investigation in this context. This study aims to interpret the evolution of slate slope deformation from long-term kinematics to short-term activity. We first observe the surficial displacement rate during the period of 2018-2020 using multi-temporal InSAR analysis. The radar satellite-based surface observation was then supplemented with numerical analysis based on the distinct element method to characterize the sub-surface gravity-driven slope movement. Our results help explain the evolution of gravitational slope deformation in slate slopes and better assess rockslide hazards transferred from GSD.

Keywords: Gravitational slope deformation, slate slope, multi-temporal InSAR analysis, distinct element modeling.

1 INTRODUCTION

Central Range slate belt is the most dynamic and has diverse topographic among the geological environments in Taiwan. The response of landforms throughout the slate belt of Taiwan to ongoing GSD is regulated by mechanical and geometric properties of the tectonic foliations. This endogenic process within the slate slopes not only dominates landscape evolution but also plays a critical role in associated large or secondary landslides. The Central Geological Survey of Taiwan has recognized over 35,000 landslides occurring in this area during 2009 Typhoon Morakot (Huang et al., 2016). The Lushan North Slope, which is located in the Chingjing region (Fig. 1), is identified as the key large landslide by the Soil and Water Conservation Bureau and often activated by torrential rainfall events. Although numerous studies contributed to the hazard mitigation in the Lushan North Slope (Chang et al., 2015; Lin et al., 2020; Lu et al., 2014), other slate slopes in the Chingjing region such as Dingyuan and Shouting domains are less discussed because lack of multi-temporal monitoring

data and analysis tools (Fig. 1b). This study integrated radar satellite-based surface observation and mechanical modeling to interpret the evolution of slate slope deformation from long-term kinematics to short-term activity in these domains. The results are expected to facilitate the assessment of rockslide activity associated with the GSD in the slate slopes.

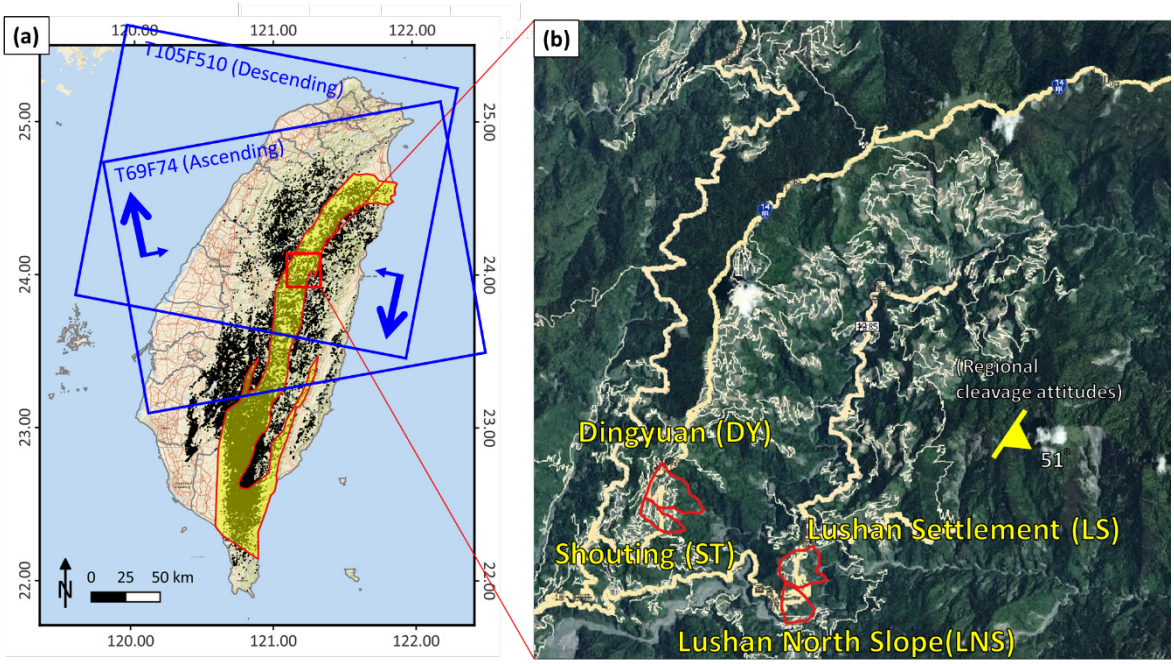

Figure 1. Location of the study area Chingjing region, Taiwan.

2 METHODOLOGY

2.1 Multitemporal InSAR analysis

The short-term activity of the slate slopes in the Chingjing region was investigated by processing multiple SAR image pairs acquired along ascending and descending orbits passes of the Sentinel-1A satellite sensor (Fig. 1). The Sentinel-1A spaceborne segment is operated by the European Space Agency (ESA) and provides C-band SAR images with short revisit time (12 days in our study area). We exploited SAR images that cover the period of 2018 – 2020 for each orbit pass (Fig. 2a). All SAR images were first processed using InSAR Scientific Computing Environment (ISCE) software developed at NASA JPL Caltech (Rosen et al., 2012). We used the Stack Sentinel module to generate SAR acquisition pairs by taking orbital data, SRTM 30m DEM, auxiliary data (Sentinel-1 instrument parameters) and bounding box into account.

To detect extremely slow slope movement within the order of mm/yr, the Persistence Scatter Interferometry (PSI) technique was adopted in this study. All Interferograms were processed through the Stanford Method for Persistent Scatterers (StaMPS) algorithm (Hooper et al., 2012). The StaMPS algorithm permits measurement of ground displacements by means of Permanent Scatterers (PS) like buildings, rock and debris. The PS is characterized by high signal-to-noise ratios that represent points on ground that return a stable signal to the satellite sensor. StaMPS reduces noise and estimates DEM correction to generate time-series PS data. As shown in Fig. 2a, we then combined ascending and descending PS data to calculate the 2D ground displacement and the dip of displacement vectors according to Eriksen et al. (2017). Considering the limitation of satellite sight in north-south direction for the Sentinel-1A sensor, this study focuses on the slate slopes that have the topographic downslope direction toward east in the study area.

2.2 Distinct element modeling

The long-term kinematics of GSD was analyzed by the 2D numerical program UDEC (Universal Distinct Element Code) with the simplified slope model. UDEC is based on distinct element method, which enables the simulation of fractured rock mass behaviors and considers the influence of discontinuities (Itasca Consulting Group, Inc., 2019). For the slate slopes facing toward east in the study area, the cleavage dip direction is parallel to the topographic downslope direction (Fig. 1). Thus, the numerical model represents the cataclinal slopes in our study area. Fig. 2b shows the geometry of the UDEC model. To cover the slate slopes at various scales, we define the range of variation of the slope geometry that is used in the following simulation (Fig. 2b). The range of variation of parameters is chosen based on field investigation and geomorphic analysis (Lin et al., 2020). The heights of the slopes range from 200 to 500 m to cover the slate slopes at various scales. The distances to the side boundaries are chosen long enough to avoid interactions with the deformation zone.

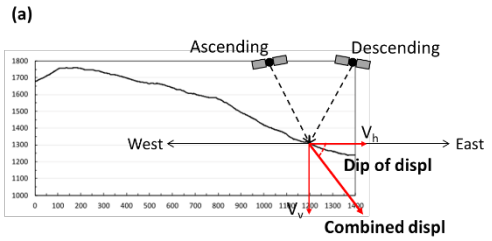

Sensor	Track	Frame	Geometry	Time interval	Images
Sentinel-1A	69	74	Ascending	2018-2020	90
Sentinel-1A	105	510	Descending	2018-2020	87

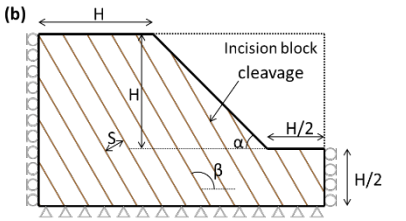

Parameter	Definition	Min. value	Max. value	Steps
α	Slope angle	25	50	5
β	Joint dip angle	60	80	10
H	Slope height	200	500	100

Figure 2. (a) Decomposition of 2D ground displacement from LOS displacement rate and radar image information; (b) Geometry of the numerical model.

3 RESULTS AND DISCUSSIONS

3.1 Short-term behaviors and activity

Figure 3a shows the estimated mean LOS velocity in the ascending tract using the PS-InSAR method. For the known GSD domains, more PS points are detected in areas where the scattering is of a "strong characteristic," i.e., areas with buildings and less vegetation. The LOS velocity data indicates that the upper sectors of the GSD domains exhibit deformation with an average velocity of 10-15 mm/yr. The PS points in each domain are selected to understand the temporal deformation trend. Time-series data shows that the GSD movement is more significant in the Dingyuan domain (Fig. 3b) compared to the Shouting domain (Fig. 3c). The negative LOS velocity represents that the deformation movement is away from the satellite, implying an eastward or subsidence displacement. In the period of 2018-2020, the cumulative LOS displacement for these GSD domains exceeded 40 mm. In addition, Fig. 3d shows that the LNS domain that is dominated by rockslide behavior (Lin et al., 2020) exhibits the greatest deformation rate of approximately 20 mm/yr in the analysis period.

To better interpret the short—term behaviors of the GSD movement, we calculated the 2D ground displacement and the dip of displacement vectors from ascending and descending LOS velocity data. Figure 4 shows that the combined velocities are generally higher in the middle GSD sectors, reaching approximately 20 mm/yr at around 1600 m height and testifying the ongoing active deformation for the entire slopes. At the upper sectors of the GSD domain, combined velocities range between 10 and 20 mm/yr. From the DY1-1' and ST1-1' profiles, we observe that the displacement vectors exhibit "dip-in" and "along slope movement" features at the upper and middle sectors of the slopes, respectively. In addition, for the LNS1-1' profile, the combined velocity fades to 0 - 5 mm/yr near the riverbed and the displacement rate vectors become "daylighting". Across the mountain crest, the

displacement rate dips to the converse side due to the variation of downslope direction. Overall, the 2D InSAR combined velocity data indicates that the three GSD domain is undergoing extremely slow deformation according to the activity classification proposed by Cruden and Varnes (1996). Judging from the steeper dip of the displacement in the upper part of the slopes, a deep basal sliding surface could be taking place along the discontinuous basal shear zones. We speculate that this may be the results of the favorable orientation of the cleavage in the slate slope, which is rotated inward and may form slide planes within the GSD domain.

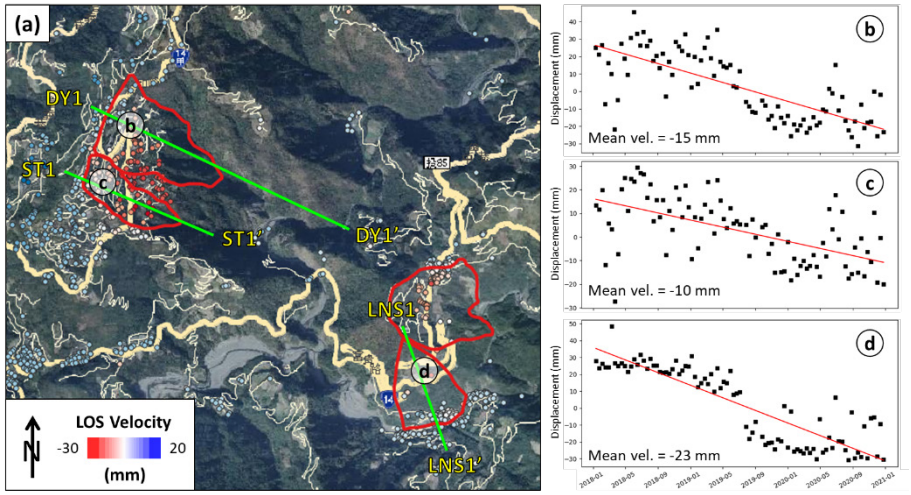

Figure 3. Results of the PSInSAR analysis. (a) LOS velocity field. (b, c, d) Time-series LOS velocities for the selected PS points in Dingyuan and Shouting domains.

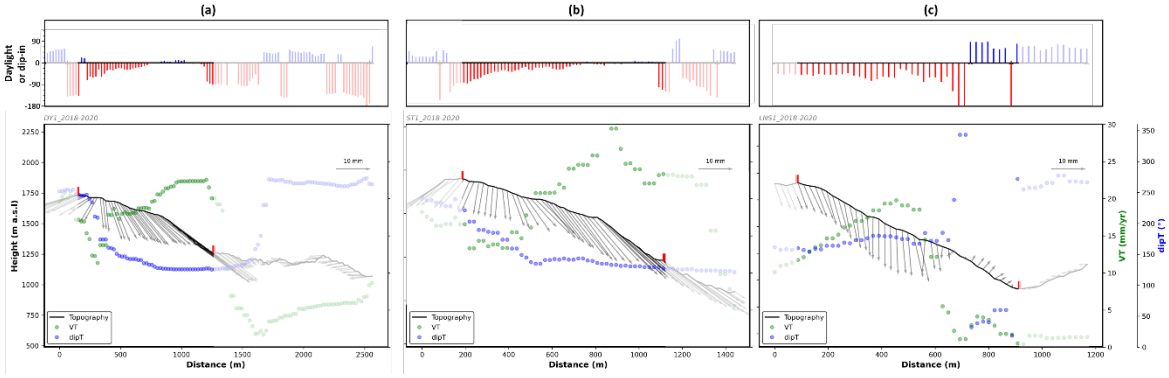

Figure 4. 2D displacement (VT) and the dip of displacement vectors (dipT) for (a) DY1-1', (b) ST1-1', and (c) LNS1-1' profiles. The data outside the domains are masked with 50% transparency.

3.2 Long-term evolution and kinematic behaviors

There are 72 simulations which have been performed with different slope geometry (Fig. 2b) to investigate the influence of slope scales in terms of GSD kinematics. All the simulations exhibit similar overall evolution over computation time-steps and kinematic behaviors. Hereafter, we present the generic behavior based on an exemplary slope ($\alpha = 40^{o}$; $\beta = 80^{o}$; $H = 300$ m). Figure 4 shows the simulation with displacement field for different model stages. A significant displacement occurs at the upper slope and shows a sign of kinematic transition to downward slope. Loading from the active wedge drives the passive wedge through the middle transition part (Fig. 4a). This kinematic movement enables basal sliding plane to be accommodated by a lower angle at the slope toe. While the high stress concentrations at the slope toe, flexural toppling occurs with progressive acceleration of the deformation (Fig. 4b). The continued deformation facilitates the coalescence of active wedge and transition part to become a sliding block. We observe that the rock mass has higher displacement

in a certain depth than the slope surface and the basal plane. The character indicates that the shear strain localization along newly formed kink bands at depths of approximately 120 m. The movement of the GSD becomes steady when the computation time-steps increases to 500000 (Fig. 4c). The basal plane of the GSD block consists of shearing along cleavage at the upper slope and shearing along rock mass from transition part to the toppling block. The thickness and volume of the GSD block is approximately 130 m and 55000 m^3, respectively.

Figure 4d shows that the GSD initiates by sliding along the cleavage at the upper slope. Meanwhile, the cleavages exhibit several counter scarps due to bulging movement in the transition part. The toppling that occurs at the slope toe results in trench terrain. The upper slope experiences a retrogressive sliding when the deformation continues (Fig. 4e). A series of scarps can be observed from foliation-parallel surfaces at the head of the GSD. The simulation also reproduces the general internal structures of the GSD, with chevron folds of cleavage at the head of the slope and overturned cleavages at its toe (Lin et al., 2020). At depths of 80 and 125 meters, two hinge lines can be identified from the S-shaped deformed rock mass, implying potential shear planes formed during the GSD process. Figure 4f shows that the cleavages above the upper hinge line remain at the dip angle of 80º and no displacement occurs along the cleavage in the same area. We conclude that the modeling indicates a two-stage kinematic behavior: first, an initiation and maturation of the damaged zone with diffuse damage and without much displacement (Fig. 4a, 5a), and second, a stage of acceleration when the damaged area connects the toe and the top of the slope (Fig. 4c, 5b). The variation of the surficial displacement vectors from the UDEC modeling are also compatible with the observation of the PSInSAR analysis, showing dip-in to daylighting feature from crest to toe (Fig. 5c).

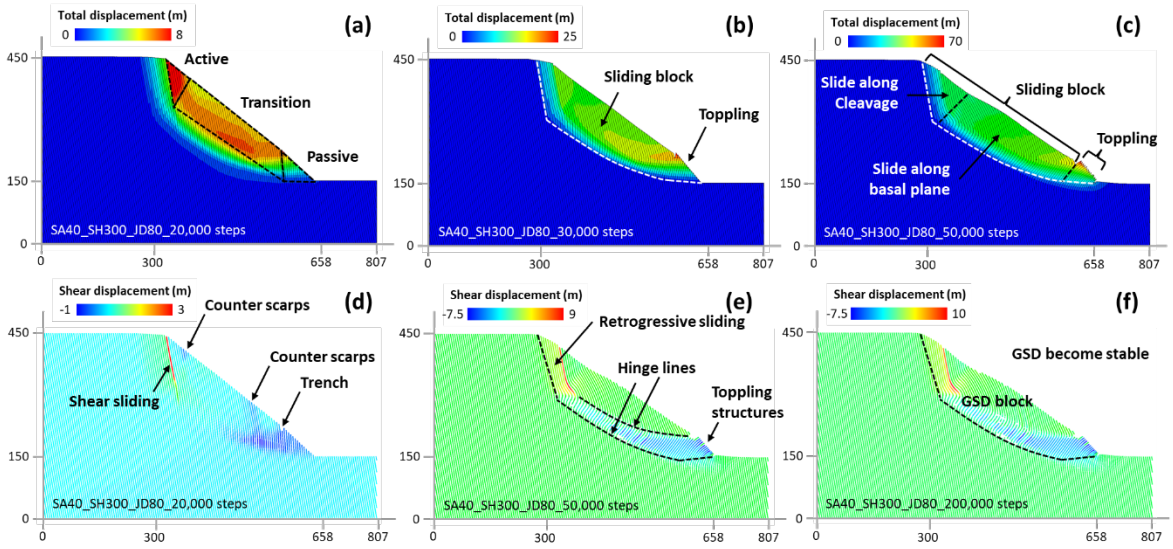

Figure 4. Results of the GSD evolution. (a)~(c) rock mass displacement and (d)~(f) cleavage displacement.

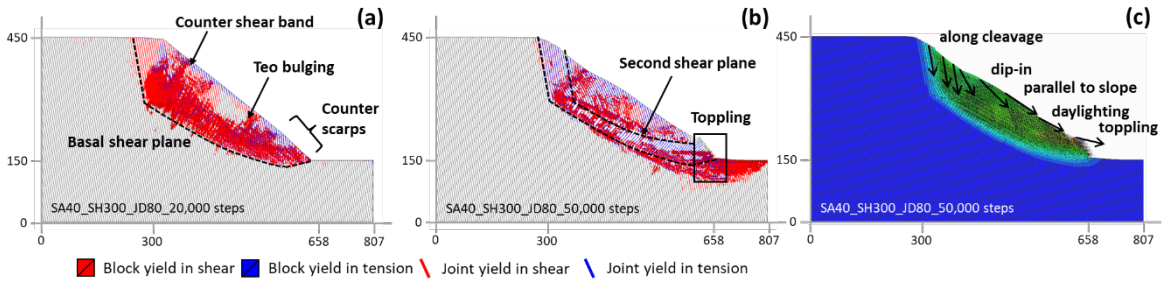

Figure 5. Distribution of the damage zone due to GSD at the numerical time-steps of (a) 20000 and (b) 50000. (c) The pattern of the surficial displacement vectors at the 50000 numerical time-steps.

4 CONCLUSIONS

This study provides novel insights into the development and present-day deformation of slate slope activity in the Chingjing region, Taiwan. The 2D PSInSAR combined data indicates that the three GSD domains are undergoing extremely slow deformation with velocity of approximately 20 mm/year. In addition, the vectors of the combined displacement data imply that the kinematic movement of recent deformation is within a rotational basal plane. On the other hand, the evolution of slow-moving GSD was simulated and raise questions concerning spatial and temporal damage patterns and timing. Based on mechanical modeling, for a slate slope with the height of 300 m, the thickness and volume of a GSD damage zone is approximately 130 m and 55000 m^3, respectively. Two hinge lines at depths of 80 and 125 meters can be identified from the S-shaped deformed rock mass, implying basal shear planes formed during the GSD process. Overall, with the multidisciplinary approach based on the integration of radar satellite analysis and mechanical modeling, more comprehensive monitoring of potential rock slope instabilities in the slate belt of Taiwan is enabled.

ACKNOWLEDGEMENTS

The authors appreciate the reports and monitoring data provided by Central of Geology, Taiwan and Land Engineering Consultants Co., LTD. We also thank the Ministry of Science and Technology, Taiwan, for financially supporting this research under Contracts MOST 111-2625-M-002-024-.

REFERENCES

Chang, K. T., Ge, L., & Lin, H. H. 2015. Slope creep behavior: observations and simulations. Environmental Earth Sciences, 73, 275-287. DOI: 10.1007/s12665-014-3423-2

Cruden, D.M. and Varnes, D.J. 1996. Landslide Types and Processes, Transportation Research Board, U.S. National Academy of Sciences, Special Report, 247, 36-75. DOI: 10.3133/fs20043072

Eriksen, H. Ø., Lauknes, T. R., Larsen, Y., Corner, G. D., Bergh, S. G., Dehls, J., & Kierulf, H. P. 2017. Visualizing and interpreting surface displacement patterns on unstable slopes using multi-geometry satellite SAR interferometry (2D InSAR). Remote Sensing of Environment, 191, 297-312. DOI: 10.1007/s00603-019-01923-4

Hooper, A., Bekaert, D., Spaans, K., & Arıkan, M. 2012. Recent advances in SAR interferometry time series analysis for measuring crustal deformation. Tectonophysics, 514, 1-13. DOI: 10.1007/s00603-019-01923-4

Huang, C., Byrne, T. B., Ouimet, W. B., Lin, C. W., Hu, J. C., Fei, L. Y., & Wang, Y. B. 2016. Tectonic foliations and the distribution of landslides in the southern Central Range, Taiwan. Tectonophysics, 692, 203-212. DOI: 10.1016/j.tecto.2016.06.004

Itasca Consulting Group, Inc. (2019) UDEC — Universal Distinct Element Code, Ver. 7.0. Minneapolis: Itasca.

Lin, H. H., Lin, M. L., Lu, J. H., Chi, C. C., & Fei, L. Y. 2020. Deep-seated gravitational slope deformation in Lushan, Taiwan: Transformation from cleavage-controlled to weakened rockmass-controlled deformation. Engineering Geology, 264, 105387. DOI: 10.1007/s00603-019-01923-4

Lu, C. Y., Tang, C. L., Chan, Y. C., Hu, J. C., & Chi, C. C. 2014. Forecasting landslide hazard by the 3D discrete element method: A case study of the unstable slope in the Lushan hot spring district, central Taiwan. Engineering Geology, 183, 14-30. DOI: 10.1016/j.enggeo.2014.09.007

Rosen, P. A., Gurrola, E., Sacco, G. F., & Zebker, H. 2012. The InSAR scientific computing environment. In EUSAR 2012; 9th European conference on synthetic aperture radar (pp. 730-733). VDE.